Electrochemical oxidation for decolorization of Rhodamine-B dye using mixed metal oxide electrode: modeling and optimization

Manisha S. Kothari and Kosha A. Shah

ABSTRACT

In the study the electrochemical oxidation process for decolorization of Rhodamine-B dye was studied using an anode coated with mixed metal oxides: TiO_2, RuO_2, and IrO_2. Batch experimental studies were conducted to assess the effect of four important performance variables, current density, electrolyte concentration, initial pH and electrolysis time, on the decolorization and energy consumption. The process was modeled using an artificial neural network. Response surface methodology using central composite design (CCD) was utilized for optimization of the decolorization process. Based on the experimental design given by CCD, the results obtained by the statistical analysis show that the electrolysis time was the most influential parameter for decolorization whereas the current density had the greatest influence on the energy consumption. According to the optimized results given by the CCD model, maximum color removal of 97% and minimum energy consumption of 1.01 kWh/m^3 were predicted in 4.9 minute of electrolysis time, using 0.031 M NaCl concentration at current density 10 mA/cm^2 and an initial pH of 3.7. A close conformity was observed between the optimized predicted results and experimental results. The process was found to be efficient and consisted of indirect chemical oxidation producing strong oxidizing agents such as Cl_2, HClO and OCl^-.

Key words | analysis of variance, central composite design, electrochemical oxidation, modeling, optimization, response surface methodology

Manisha S. Kothari
Kosha A. Shah (corresponding author)
Civil Engineering Department, Faculty of Technology and Engineering,
The Maharaja Sayajirao University of Baroda,
Vadodara 390001,
India
E-mail: *kosh482000@yahoo.co.in*

INTRODUCTION

A wide range of industries such as textile, pulp and paper manufacturing, distilleries and tanneries use various types of dyes (Martínez-Huitle & Brillas 2009). Dyes have undesirable color, high toxicity and persistence. In addition, many dyes are recalcitrant in nature. Various conventional treatment methods such as physical methods, which include adsorption, irradiation, membrane filtration and ion exchange; chemical methods such as chemical coagulation; and biological methods, which include biosorption, aerobic processes and anaerobic processes, are used for the treatment of dye wastewaters (Forgacs *et al.* 2004). Due to the toxic and obstinate nature of some dyes, these methods are not effective for the removal of such dyes. These methods have certain inherent limitations such as unsatisfactory treatment, large sludge generation problems and introduction of secondary pollution (Gutierrez & Crespi 1999; Robinson *et al.* 2001; Naim & El Abd 2002). Recently advanced oxidation processes (AOPs) have become promising techniques to eliminate these disadvantages of conventional treatment processes (Simond *et al.* 1997; Hao *et al.* 2000). AOPs are advantageous methods as they cause complete degradation of pollutants with no generation of pollutants (Kötz *et al.* 1991; Stucki *et al.* 1991). The principle reaction that takes place during AOPs is the generation of a very strong oxidizing agent, hydroxyl radicals (•OH), that oxidizes complex organic as well as inorganic compounds.

Among the AOPs, electrochemical oxidation processes are gaining attention due to their effectiveness, automation capacity, clean reagent usage and versatility (Bedolla-Guzman *et al.* 2016). Most commonly, electrochemical oxidation processes involve oxidation of organic compounds at the anode or formation of strong oxidizing species like hydroxyl radicals (Panizza & Cerisola 2009).

A schematic of the electrochemical oxidation process is shown in Figure 1. There are two mechanisms involved in

doi: 10.2166/wst.2020.151

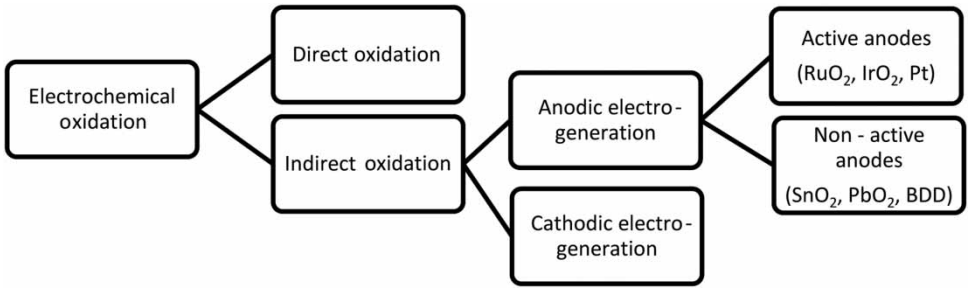

Figure 1 | Schematic electrochemical oxidation process.

the electrochemical oxidation process, namely, (i) direct oxidation and (ii) indirect oxidation. The process was described by Comninellis & Chen (2010).

In direct oxidation, oxidation of the pollutant occurs by direct electron exchange between the anode and the organic pollutant without the participation of mediators.

In indirect oxidation, mediative species are generated, which act as mediator for the electron transfer between the anode and the organic pollutant. The mediator is generated by either the anodic or cathodic electrogeneration process (Panizza & Cerisola 2009). The anodic electrogeneration processes are dependent on type of the anode material. There are two types of anode material: active and non-active. In active anodes (e.g., RuO_2, IrO_2, Pt), the oxidation of organic compound is soft and selective. In contrast, for non-active anodes (e.g., SnO_2, PbO_2, boron doped diamond (BDD)), the oxidation is severe and non-selective, resulting in complete mineralization of the organics (Martinez-Huitle & Panizza 2018).

In both the active and non-active anodes, a strong oxidant, •OH, is formed, on the anode surface (M) (Equation (1)).

For active anodes, the adsorbed hydroxyl radicals forming M(•OH) are partially converted into a weaker oxidizing agent, a metal oxide (MO) (Equation (2)) (Fajardo *et al.* 2019). The MO acts as mediator, causing the selective oxidation of the organic pollutant (R) as shown in Equation (3).

For non-active anodes, the oxidation of organic pollutant is achieved by physisorbed hydroxyl radical to complete mineralization as shown in Equation (4).

$$M + H_2O \rightarrow M(^{\bullet}OH) + H^+ + e^- \quad (1)$$

$$M(^{\bullet}OH) \rightarrow MO + H^+ + e^- \quad (2)$$

$$MO + R \rightarrow M + RO \quad (3)$$

$$M(^{\bullet}OH) + R \rightarrow M + CO_2 + H_2O + H^+ + e^- \quad (4)$$

Simultaneously, active chlorine-based oxidizing mediators, such as chlorine gas (Cl_2), hypochlorous acid ($HClO^-$) and hypochlorite ion (ClO^-), are generated from the chlorides present inherently or introduced as an electrolyte (Equations (5)–(8)) (Martinez-Huitle & Panizza 2018).

$$2Cl^- \; Cl_{2(el)} + 2e^- \quad (5)$$

$$Cl_{2(el)} \; Cl_{2(sol)} + 2e^- \quad (6)$$

$$Cl_{2(sol)} + H_2O \rightarrow HClO + Cl^- + H^+ \quad (7)$$

$$HClO \rightarrow \; + H^+ + ClO^- \quad (8)$$

Many researchers have used the electrochemical oxidation technique for treatment of landfill leachate (Li *et al.* 2013), dye wastewater, (Esquivela *et al.* 2009), phenolic wastes (Canizares *et al.* 2005), and polyhydroxybenzenes (Canizares *et al.* 2004).

The efficiency of the electrochemical process depends upon the oxygen evolution potential (OEP) of the anode material chosen. Many researchers have assessed the efficiency of different metal oxide coatings on titanium (Ti) metal for anodes, such as RuO_2 (Mohan *et al.* 2001), SnO_2 (Stucki *et al.* 1991; Comninellis & Pulgarin 1993; Chen *et al.* 2003), PbO_2 (Kawagoe & Johnson 1994; Gherardini *et al.* 2001; Awad & Galwa 2005) and BDD electrode (Mohan *et al.* 2001; Chen *et al.* 2003; Mohan & Bala Subramanian 2006). BDD anodes suffer from the limitation of high initial cost and hence limited application on large scale industrial wastewater treatment, whereas single metal coatings (RuO_2, SnO_2, PbO_2) are known to have lower stability and efficiency. Dimensionally stable anodes are made by coating a layer of mixed metal oxides on a base metal. This study aims to use a mixture of active metal oxides which have excellent oxidative capacity and lower cost, making them promising anodes for industrial

wastewater treatment applications. Further, the goal is to model and optimize the electrochemical process for achieving reduction in cost and time. An artificial neural network (ANN) was used for modeling the process. The stimulated data from ANN model was fed into the RSM software for optimization of the process. In the ANN network, the inputs are fed by the user. These inputs are multiplied by their weights to enable strong signals, which pass through a mathematical function to produce the output. Adjusting of weights to process the information is called learning or training. Once a neural network is trained, it can deliver outputs for similar types of problems. Presently, an ANN which learns using the back propagation algorithm for learning the appropriate weights is one of the most common models used in ANN. Two types of ANNs commonly used are (1) Kohonen self organizing mapping and (2) multilayered feed forward neural network trained by back propagation algorithm. In the back propagation algorithm, as we simulate the network with input and output data, the network trains itself and produces the predicted output through hidden layers. The difference between the observed and the predicted output is the error. In the back propagation algorithm, the attempt is made to minimize this error by assigning appropriate weights to the input variables through training of the fed data. The activation function of the artificial neurons in ANNs implementing the back propagation algorithm is a weighted sum. The activation depends only on the inputs and the weights.

In this study, an active anode was prepared by mixing the metal oxides RuO_2, TiO_2, and IrO_2 and coating the mix on both sides of a Ti plate. Oxides of various metals such as RuO_2, TiO_2, IrO_2 have high conductivity and OEP: RuO_2 (1.47 V vs SHE), TiO_2 (1.22 V vs SHE), IrO_2 (1.52 V vs SHE). Rhodamine B dye is selected as a model dye because it is carcinogenic, persistent and difficult to remove. Rhodamine-B is a xanthene cationic dye and recalcitrant. It is used in paper printing, textile dying and as food additive.

MATERIALS AND METHOD

Materials

All analytical grade chemicals were used in the experiments as received. Distilled water was used to prepare all the aqueous solutions. Rhodamine-B dye ($C_{28}H_{30}N_2O_3$) was purchased from a local chemical laboratory with 99% purity. Table 1 shows the characteristics of Rhodamine-B dye. The chemical structure of the dye is shown in Figure 2. Stock solution of 10,000 mg/L was prepared and appropriate solutions were prepared by diluting for experimental studies. Initial conductivity of a 250 mL Rhodamine-B solution (Rhodamine-B + 0.03 M NaCl) was found to be 3.1 mS/cm. Mixed metal oxide (MMO) used in the study was fabricated by a local engineering company.

Table 1 | Characteristic of Rhodamine-B dye

Pollutant name	Rhodamine-B
Molecular formula	$C_{28}H_{30}N_2O_3$
Solubility in water	15,000 mg/L
Molar mass	479.02 g/mol
Maximum absorbance (λmax)	554 nm

Experimental procedure and analytical techniques

The electrochemical cell with a working volume of 250 mL, consisting of an undivided reactor made up of polyacrylic having dimensions of 7 cm × 6.5 cm × 7 cm was used for the experiments. A commercially available Ti plate coated with mixed metal oxides (TiO_2, IrO_2, RuO_2) was used as anode. A stainless steel plate was used as cathode, both the plates having dimensions of 5 cm × 5 cm. Both anode and cathode are positioned upright and parallel to each other in batch operation. The two parallel electrodes had an inter-electrode spacing of 6 cm. DC current was supplied to the synthetic dye solution with a DC power supply (Toschon industries, India). A magnetic stirrer (Janki Impex, India) was used for thorough mixing of the aqueous medium. Preliminary experiments were carried out at 30 °C temperature. The UV-Vis spectra of the samples were recorded from 200 to 900 nm using a UV-Vis spectrophotometer (Shimadzu UV-1800) (APHA *et al.* 1995). At fixed time interval of 1 min, samples were withdrawn, filtered (Whatman No. 1 filter paper) and analyzed for color removal. The color removal of Rhodamine-B was

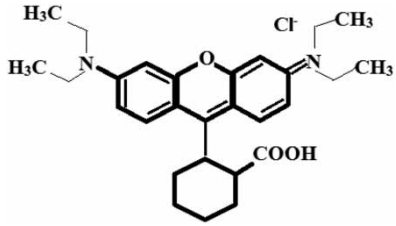

Figure 2 | Chemical composition of Rhodamine-B dye.

determined by measuring the absorbance at 554 nm wavelength. A schematic diagram of the batch reactor set-up is shown in Figure 3. Experimentally, color removal is calculated as percentage by Equation (9).

$$\text{Color removal}(\%) = \left[\frac{\text{Ab}_0 - \text{Ab}_t}{\text{Ab}_0}\right] \times 100 \quad (9)$$

where Ab_0 is the initial absorbance of the solution at the maximum wavelength ($\lambda\text{max} = 554$) before electrolysis and Ab_t is the final absorbance after an electrolysis time t, respectively. The energy consumption (kWh/m^3) of treated wastewater was calculated using Equation (10) (Martínez-Huitle & Brillas 2009). The cell voltage and the current do not fluctuate significantly with time during the electrolysis and hence average values are considered (Rocha *et al.* 2012).

$$\text{Energy consumption} = \frac{[\text{v} \times \text{A} \times \text{t}]}{1000 \times \text{V}_s} \quad (10)$$

where t is the electrolysis time in hours, V_s is the sample volume in cubic metres, v is the cell voltage in volts and A is the current in amperes.

Scanning electron microscopy (SEM) analysis was performed with a JEOL scanning electron microscope with Oxford EDS system to study the physical structure. Energy dispersive X-ray spectroscopy (EDS) analysis was done to determine chemical composition of the MMO electrode.

Artificial neural network modeling

In this study, the ANN model was designed with sigmoid transfer functions. Initial pH, electrolysis time, electrolyte concentration and current density were selected as input variables, and percentage color removal and electrical energy consumption as output variables. A total of 50 experimental data sets from preliminary studies were used to feed the ANN structure. The data sets were divided into training, validation and test subsets, containing 70%, 20% and 10% of samples, respectively. MATLAB (The Mathworks, Inc., ver. 7.6) computing environment was chosen to generate

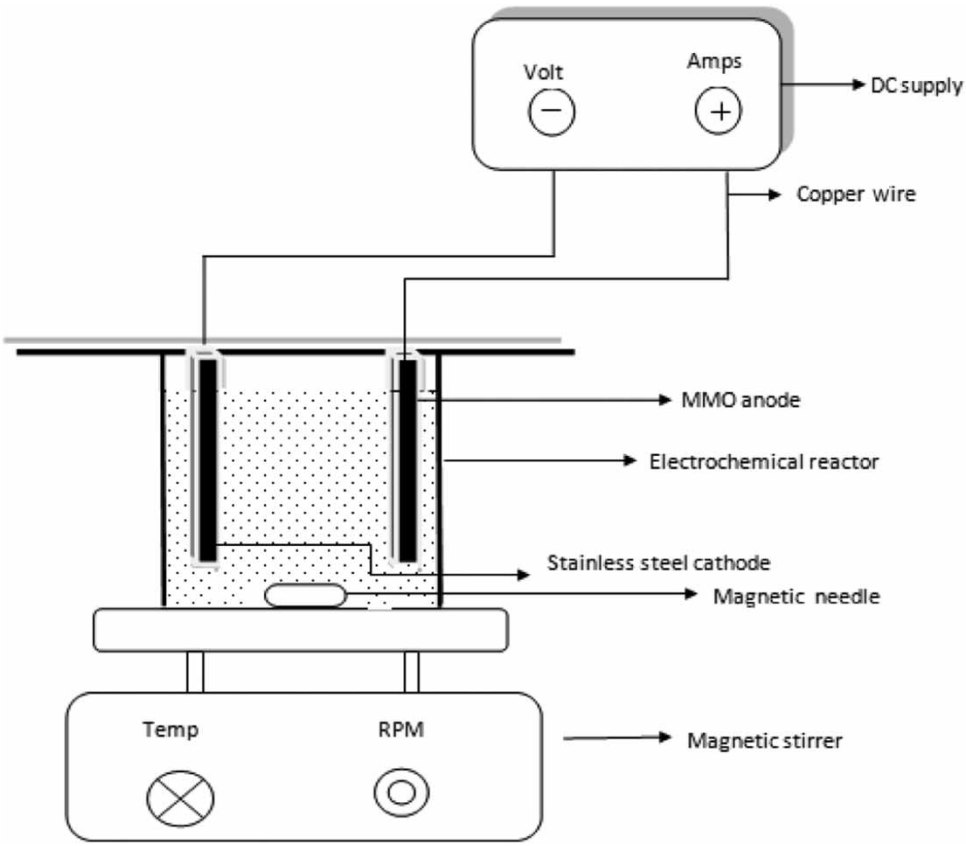

Figure 3 | Schematic diagram of the reactor set-up.

the neural network model from the data. Pre-processing of the inputs and output was done by randomization to make the neural network training more efficient. Hyperbolic tangent 'TANSIG' being a sigmoid transfer function was chosen for the input to hidden layer mapping while a linear transfer function 'PURELIN' was chosen for the hidden layer to the output layer mapping.

Response surface methodology

After modeling of the experimental process, a statistical tool, response surface methodology (RSM) was employed for model representation and optimization of the electro-oxidation process. To find the optimum conditions, the central composite design (CCD) was preferred as it is best for a series of experiments. The range of levels for the central composite experimental design was decided based on preliminary experiments. The rotatable CCD experimental design was prepared with four independent variables and two response variables, at five levels, constituting 30 experiments, by the means of the Design Expert software (version 8.0). The independent variables selected for this experiment were electrolysis time (X_1), initial pH (X_2), electrolyte concentration (NaCl) (X_3), and current density (X_4). Percentage color removal and energy consumption were selected as response variables. Actual values of the variables are shown in Table 2.

The relationship among the four independent variables and responses is revealed as an empirical quadratic polynomial equation, which is shown as Equation (11).

$$y = \alpha_0 + \sum_{i=1}^{k} \alpha_i x_i + \sum_{i=1}^{k} \alpha_{ii} x_i^2 + \sum_{i-1}^{k-1} \sum_{j=1}^{k} \alpha_{ij} x_i x_j + \varepsilon \qquad (11)$$

where α_0 is a constant, α_i is the linear coefficient, α_{ii} is the second-order coefficient, α_{ij} is the interaction coefficient, y indicates the response variable, x_i and x_j are the coded values of the independent variables, and k indicates the number of independent variables (Iranpour *et al.* 2018).

Table 2 | Independent variables with range and magnitude

	Range and magnitude				
Independent variables	$-\alpha$	**−1**	**0**	**1**	$+\alpha$
Electrolysis time (X_1, min)	1	2	3	4	5
Initial pH (X_2)	1	3	5	7	9
Electrolyte conc. (NaCl) (X_3, M)	0.01	0.02	0.03	0.04	0.05
Current density (X_4, mA/cm^2)	5	10	15	20	25

RESULTS AND DISCUSSION

Characterization of MMO electrode

Figure 4 shows the SEM image for the surface of MMO electrode. In the SEM images of the electrode, a cracked-mud structure with flat surfaces was found. The cracked-mud

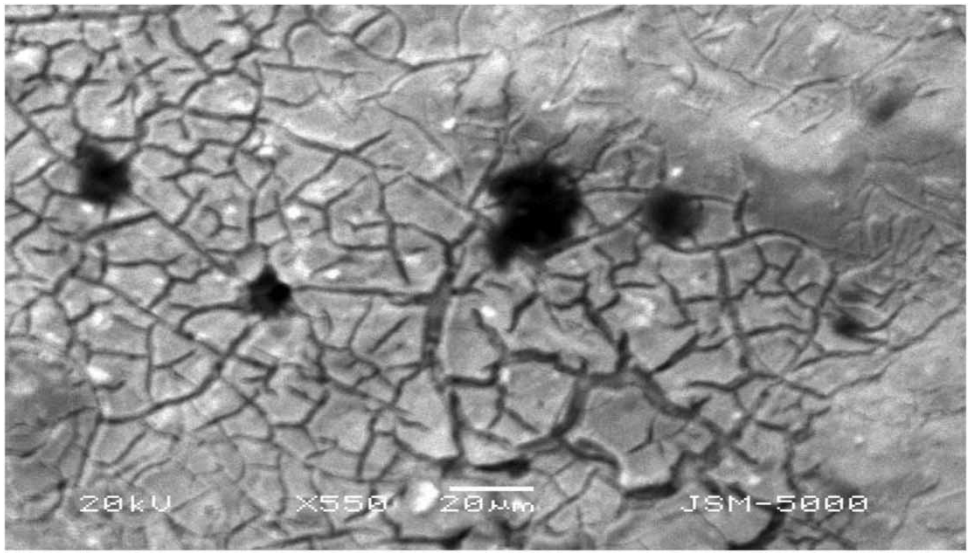

Figure 4 | SEM image of MMO electrode.

structure shows coating of MMO on the Ti plate and may be indicative of adherent characteristics of the mixed oxides during the preparation phase (Moradi & Dehghanian 2014). Black spots were observed which may be formed due to excessive cracking and subsequent abrasion of the coat at some locations on the plate.

EDS is done to assess the content of each element in the coating of electrode. Figure 5 shows the EDS image of the MMO electrode. The image clearly shows the peaks for four elements: Ru, Ir, Ti and O, which are observed in their oxides form. Table 3 shows the mass fraction of elements in the electrode coating.

Table 3 | Mass fraction of elements in electrode coating

Element	Weight %
O	41.77
Ti	36.36
Ir	4.02
Ru	17.85

ANN architecture

Mapping and the final selected network architecture were trained for 2,000 iterations. A number of training runs were performed to look out for the best possible weights in the error back propagation framework. To obtain optimum number of neurons, a series of topologies were used, in which the number of neurons was varied from 11 to 15. Mean square error was an error function in these topologies. The back propagation algorithm minimized the mean square error between the observed and the predicted values. Number of neurons of the hidden layer was noted with minimum possible mean square error. The optimized neurons for the process were 12 with mean square error of 0.5. The best validation performance was obtained at epoch 4. The regression plots of the trained network are shown in Figure 6. The overall regression coefficient obtained was 0.9856, with regression coefficients for training, validation and test of all data sets as 0.9934, 0.9791, and 0.9583 respectively. These values confirm that the ANN model was trained successfully and is ready to simulate the outputs from a given set of inputs. Figure 7 shows the schematic architecture of the ANN structure formed by modeling the process. The ANN performance plot is shown in the Supplementary Material (Figure S1).

Experimental design analysis

The experimental design was generated in the RSM software by feeding the input independent parameter range from Table 2. The responses in the design were fed into the RSM experimental design from the stimulated ANN response data. Table 4 shows the experimental and predicted responses of ANN and RSM for the statistical combinations of independent variables, namely, electrolysis time (X_1), initial pH (X_2), electrolyte concentration (NaCl) (X_3), and current density (X_4). RSM predicted versus actual plots are shown in Figures S2 and S3 (Supplementary Material). It is observed from Table 4 that the experimental and predicted values are close for a majority of runs. However, the predicted values of runs 5, 23 and 24 show significant variation from experimental values. These points are possible

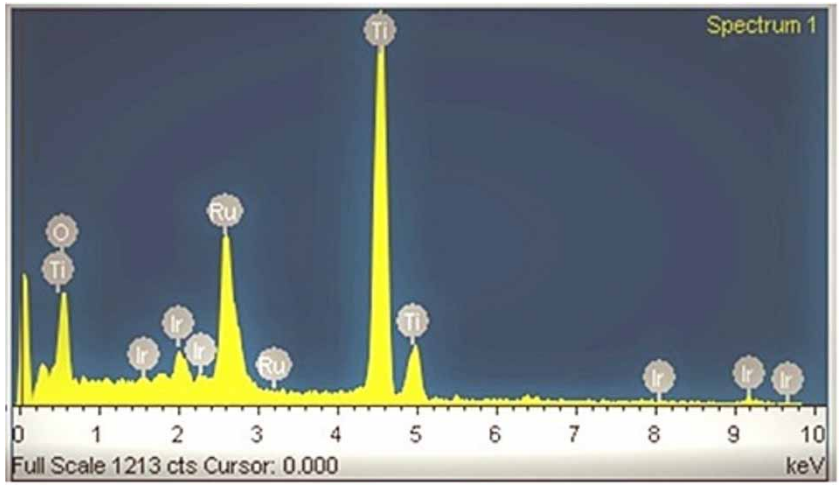

Figure 5 | EDS image of MMO electrode.

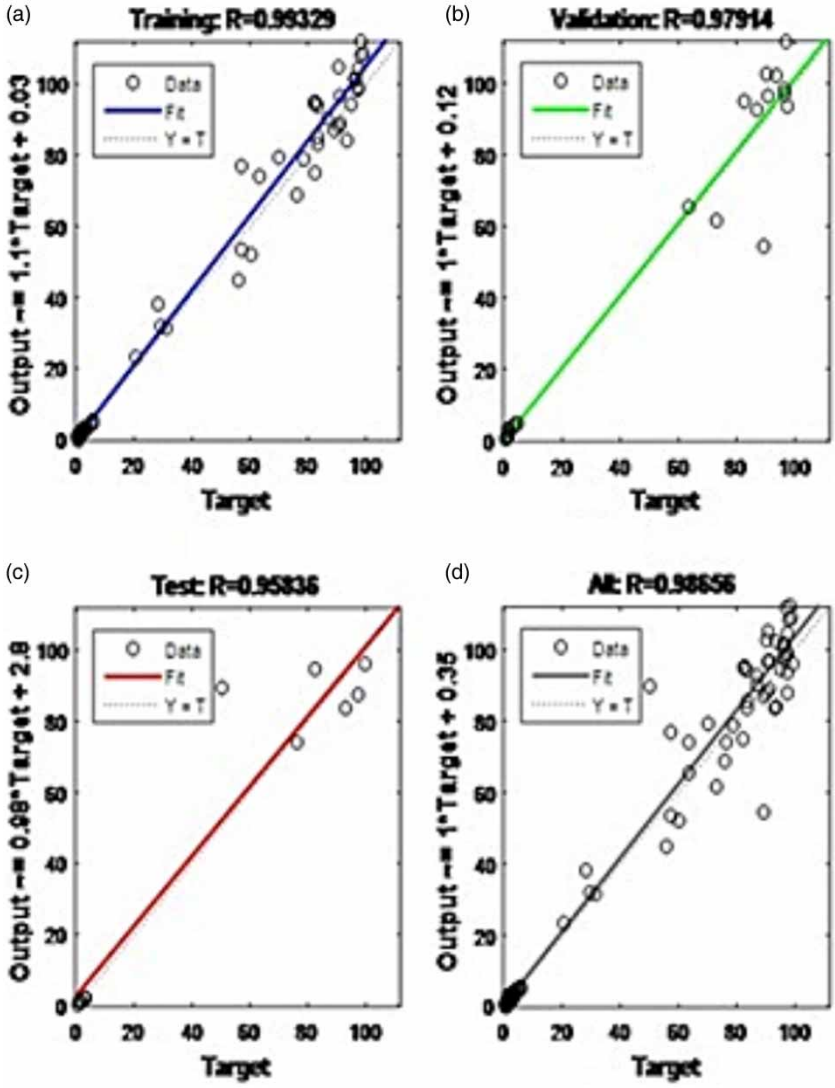

Figure 6 | Regression plots for (a) training, (b) validation, (c) test and (d) all.

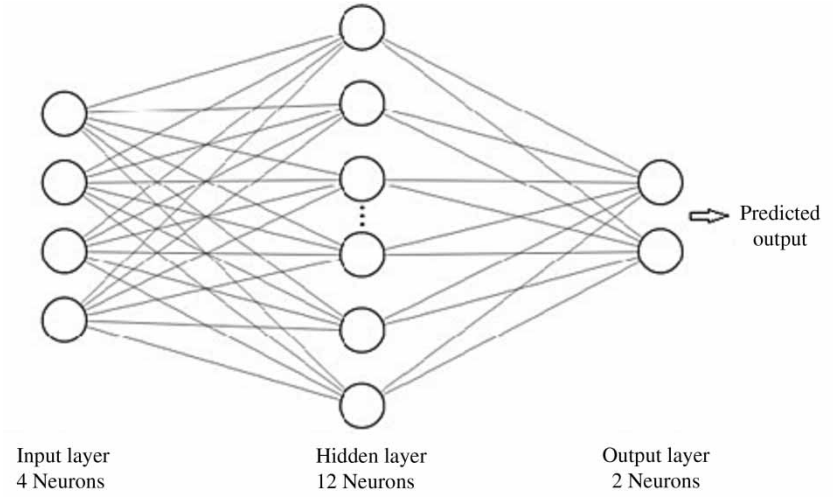

Figure 7 | ANN schematic architecture.

Table 4 | Experimental and predicted values of response variables for the electrolysis process

Run no.	Electrolysis time (min) (X_1)	Initial pH (X_2)	Electrolyte conc. NaCl (M) (X_3)	Current density (mA/cm^2) (X_4)	Color removal (Y_1, %)			Energy consumption (Y_2,kWh/m^3)		
						Predicted value			Predicted value	
					Exp. value	ANN	RSM	Exp. value	ANN	RSM
1	2	3	0.02	10	63.6	61.7	63.98	0.6	0.61	0.54
2	4	3	0.02	10	97.54	95.7	95.90	1.2	1.11	1.26
3	2	7	0.02	10	28.09	26.1	28.08	0.6	0.59	0.51
4	4	7	0.02	10	78.87	79.0	78.05	1.2	1.24	1.25
5	2	3	0.04	10	83.59	83.22	80.67	0.36	0.49	0.54
6	4	3	0.04	10	97.31	95.53	97.16	0.72	0.69	0.64
7	2	7	0.04	10	57.14	55.21	55.65	0.36	0.39	0.52
8	4	7	0.04	10	93.24	92.12	90.19	0.72	0.66	0.63
9	2	3	0.02	20	91.15	91.1	90.84	2.3	2.1	2.35
10	4	3	0.02	20	99.06	98.20	102.87	4.6	4.29	4.39
11	2	7	0.02	20	63.29	64.21	65.76	2.3	2.6	2.34
12	4	7	0.02	20	96.29	95.55	95.84	4.6	4.29	4.39
13	2	3	0.04	20	96.46	97.01	99.60	1.33	1.2	1.24
14	4	3	0.04	20	99.56	98.31	96.20	2.6	2.5	2.66
15	2	7	0.04	20	87.12	86.02	85.40	1.33	1.2	1.24
16	4	7	0.04	20	98.11	99.21	100.05	2.66	2.5	2.67
17	3	5	0.03	15	82.53	83.04	82.53	1.43	1.4	1.43
18	5	5	0.03	15	95.14	95.47	96.47	2.37	2.4	2.53
19	3	5	0.03	15	82.53	83.04	82.53	1.43	1.4	1.43
20	3	9	0.03	15	89.26	88.25	90.30	1.43	1.4	1.50
21	3	5	0.01	15	75.25	75.42	73.01	2.55	2.6	2.69
22	3	5	0.05	15	90.64	91.57	93.92	1.05	0.99	0.97
23	3	5	0.03	5	45.91	52.10	50.23	0.2	0.19	0.08
24	3	5	0.03	25	90.24	88.9	86.95	3.75	3.5	3.93
25	3	5	0.03	15	82.53	83.04	82.53	1.43	1.4	1.43
26	1	5	0.03	15	50.2	51.23	49.90	0.47	0.45	0.37
27	3	5	0.03	15	82.53	83.04	82.53	1.43	1.4	1.43
28	3	5	0.03	15	82.53	83.04	82.53	1.43	1.4	1.43
29	3	5	0.03	15	82.53	83.04	82.53	1.43	1.4	1.43
30	3	5	0.03	15	82.53	83.04	82.53	1.43	1.4	1.43

outliers. Subsequent regression models were generated by the experimental design, demonstrating the relationship between independent variables and the response variables.

Table 5 shows the analysis of variance (ANOVA), a statistical analysis result of the process generated from RSM. From the ANOVA table (Table 5) R^2 values, 0.98 and 0.99 for color removal and energy consumption respectively, are close to 1 implying that 98% and 99% variation in responses, i.e., color removal and energy consumption, respectively is due to the independent variables selected (Iranpour *et al.* 2018). The *p*-value, less than 0.05 for the model and the independent variables, indicates that all the process parameters, namely, electrolysis time, initial pH, electrolyte concentration and current density, are significant for color removal but for the energy consumption all parameters except initial pH are significant. The F-value indicates that electrolysis time is the most influential parameter followed by current density, initial pH, and

Table 5 | ANOVA

		F-value		p-value		
Source	**Degrees of freedom**	**Color removal %**	**Energy consumption**	**Color removal %**	**Energy consumption**	
Model	14	58.77	138.63	< 0.0001	< 0.0001	Significant
X_1	1	287.83	357.52	< 0.0001	< 0.0001	
X_2	1	104.80	0.0192	< 0.0001	0.8916	
X_3	1	96.06	228.10	< 0.0001	< 0.0001	
X_4	1	178.95	1138.92	< 0.0001	< 0.0001	
$X_1 X_2$	1	28.83	0.0116	< 0.0001	0.9157	
$X_1 X_3$	1	21.07	19.76	0.0004	0.0004	
$X_1 X_4$	1	34.99	89.56	< 0.0001	< 0.0001	
$X_2 X_3$	1	10.46	0.0116	0.0056	0.9157	
$X_2 X_4$	1	10.36	0.0116	0.0057	0.9157	
$X_3 X_4$	1	5.56	63.33	0.0323	< 0.0001	
X_1^2	1	10.18	0.0516	0.0061	0.8232	
X_2^2	1	65.06	0.3153	< 0.0001	0.5822	
X_3^2	1	7.24	15.00	0.0168	0.0013	
X_4^2	1	24.91	30.83	0.0002	< 0.0001	
R^2		0.9865	0.9918			

electrolyte concentration for color removal. The order of influence for energy consumption is current density followed by electrolysis time and electrolyte concentration and lastly initial pH. The interaction of all the parameters, electrolysis time, initial pH, electrolyte concentration and current density, with each other is significant for color removal. For energy consumption, interaction of electrolysis time with electrolyte concentration, electrolysis time with current density, and electrolyte concentration with current density is significant. Equations (12) and (13) show the quadratic model for the responses, i.e, color removal and energy consumption in terms of coded factors with only significant factors.

$$\begin{aligned}\text{Color removal}\,(\%) = {} & -82.53 + 11.64\,(X_1) - 8.31\,(X_2) \\ & + 6.73\,(X_3) + 9.18\,(X_4) + 4.51\,(X_1)(X_2) - 3.86\,(X_1)(X_3) \\ & - 4.97(X_1)(X_4) + 2.72\,(X_2)(X_3) + 2.71\,(X_2)(X_4) \\ & - 1.98\,(X_3)(X_4) - 2.04\,(X_1^2) + 6.70\,(X_2^2) \\ & - 1.72(X_3^2) - 3.18\,(X_4^2)\end{aligned} \tag{12}$$

$$\begin{aligned}\text{Energy consumption}\left(\text{kWh/m}^3\right) = {} & 1.43 + 0.5383(X_1) \\ & - 0.43\,(X_3) + 0.9608\,(X_4) - 0.1550\,(X_1)(X_3) + 0.3300\,(X_1)(X_4) \\ & - 0.2775\,(X_3)(X_4) + 0.1009\,(X_3^2) + 0.1447\,(X_4^2)\end{aligned} \tag{13}$$

Effect of independent variables on color removal

Figure 8 shows the response plot for the interactive effect of two independent variables with the other two independent variables constant and at central value in accordance with Table 2. The response surface plot for the effect of current density along with electrolyte concentration at initial pH 5 and electrolysis time of 3 minutes is shown in Figure 8(a). From the figure it can be noticed that with increase in electrolyte concentration, color removal increases, when the initial pH and electrolysis time are constant and are at central value. This is because with the increase in the electrolyte (NaCl), more chloride ions (Cl^-) are generated, which further oxidize to chlorine (Cl_2) at the anode. The production of Cl_2 or hypochlorites (HClO) in the bulk solution increases the oxidation efficiency. Also it is observed that decolorization efficiency increases with increase in current density because of more production of •OH radicals during the process. Identical results were reported by Baddouh *et al.* (2018). Additional interactive plots are shown in Figures S4, S5 and S6 (Supplementary Material).

The response surface plot for the effect of initial pH along with electrolysis time at current density 15 mA/cm^2 and electrolyte concentration 0.03M is shown in Figure 8(b). The figure reveals that with increase in pH the color removal decreases, and with increase in electrolysis time

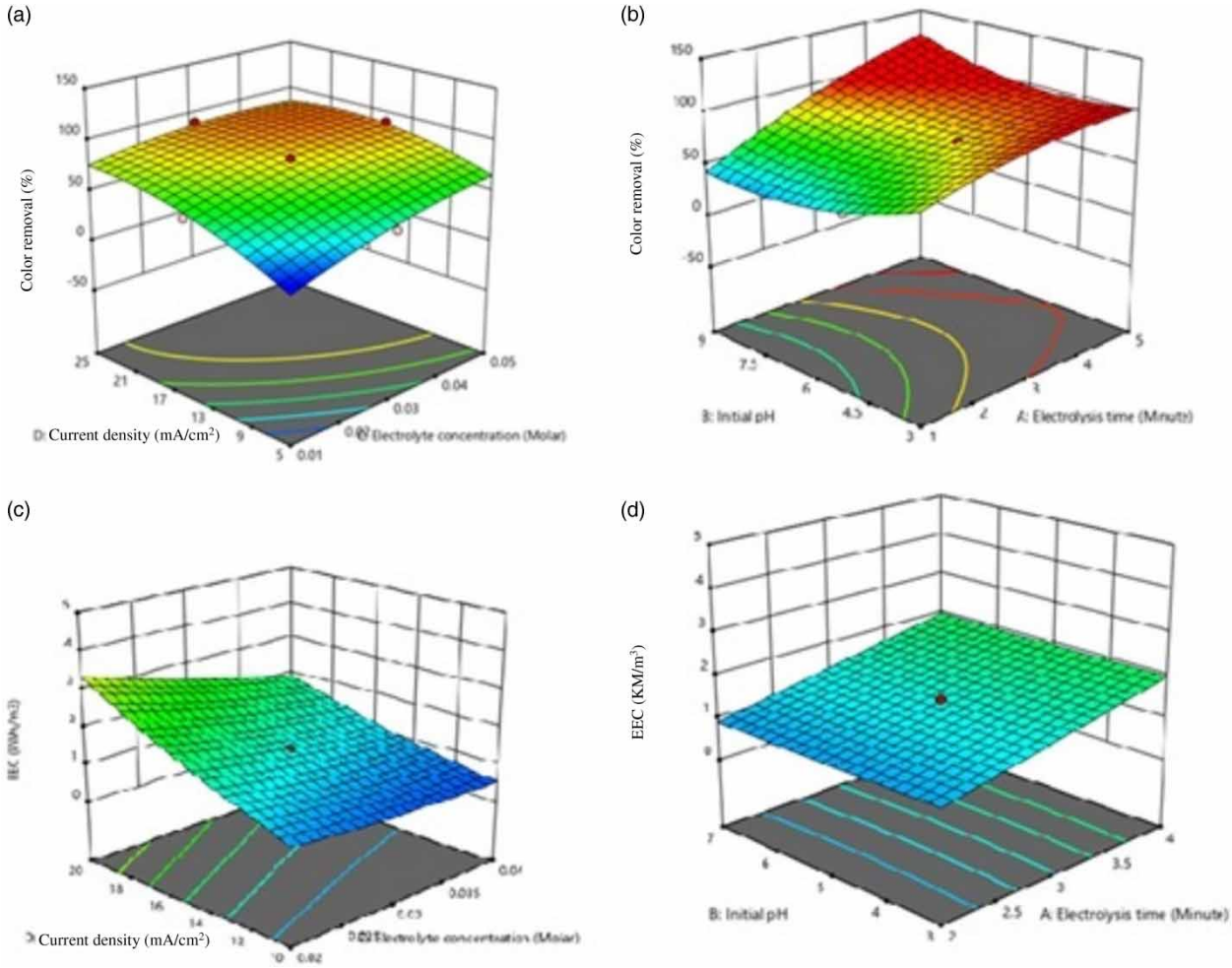

Figure 8 | Response surface plot for effect of (a) current density with electrolyte concentration on color removal, (b) initial pH with electrolysis time on color removal, (c) current density with electrolyte concentration on energy consumption and (d) initial pH along with electrolysis time on energy consumption.

color removal increases with constant electrolyte concentration and current density. Faster decolorization was observed at pH of 3 and 5 as a result of the key reaction of indirect chlorine oxidation because of efficient formation of HOCl and Cl_2 in acidic medium. Hypochlorite (OCl^-) ions are present in higher amount than other chlorine species at higher pH. Lower oxidation potential of OCl^- ions, in comparison with Cl_2 and HOCl, is the reason for slow decolorization in alkaline solution. Additionally, the Rh-B is known to have negative electrical property in alkaline solutions (Rajkumar & Kim 2006; Rajkumar & Muthukumar 2012; Baddouh *et al.* 2018). As a result, the dye molecules tend to compete with the chloride ions for the adsorption sites on the anode surface and thereby adversely affect the production of active chlorine. Similar results were obtained by Rajkumar & Muthukumar (2012).

Effect of independent variables on energy consumption

The response surface plot for the effect of current density with electrolyte concentration at initial pH 5 and electrolysis time of 3 minutes is shown in Figure 8(c). It is quite clearly observed that with increasing current density, the energy consumption increased during electrolysis because energy consumption is directly related to the applied current. Similar results were obtained by Rocha *et al.* (2012). With increase in electrolyte concentration, energy consumption decreases significantly because of increased generated ions enhancing the conductivity. The response surface plot for the effect of initial pH with electrolysis time at current density 15 mA/cm^2 and electrolyte concentration 0.03 M is shown in Figure 8(d). Initial pH seems to have a negligible

effect on energy consumption. The energy consumption increased with increase in electrolysis time.

Optimization of the decolorization process

The optimization results of RSM design using CCD representation predicts minimum energy consumption of 1.01 kWh/m^3 and 97% maximum color removal at current density of 10 mA/cm^2, initial pH of 3.7 and 0.031 M NaCl concentration at 4.9 minutes. Optimized results were validated by experiments and the experimental value of color removal and energy consumption was 96.74% and 1.2 kWh/m^3, error being 0.26% and 0.19% between experimental and predicted values respectively. Fourier transform infrared spectroscopy results of dye before treatment and after treatment are shown in Figures S7 and S8 (Supplementary Material).

CONCLUSION

In the present study, decolorization of Rhodamine-B dye from synthetic wastewater has been studied using an anode prepared of Ti plate coated with MMO (TiO_2, RuO_2, IrO_2) and a cathode made of stainless steel plate. It was found that this MMO anode had excellent oxidation capacity for decolorization of recalcitrant and persistent Rhodamine-B dye. The factors affecting the decolorization mechanism and the energy consumption were electrolysis time, initial pH, current density and electrolyte concentration. The findings show that the oxidation process follows indirect oxidation in the bulk. The presence of NaCl is responsible for the production of oxidative species such as Cl_2, HClO and OCl^-, resulting in highly efficient oxidation. The electrochemical oxidation process was modeled using an ANN for Rhodamine-B dye decolorization and energy consumption. The ANN model developed is ready to simulate the outputs from a given set of inputs. The ANN model can be used for similar industrial wastewater treatment applications with the advantage of avoiding the trial and error experimental work. Optimization of the process was carried out using RSM to delineate the effects of different process parameters on the oxidation process. The quadratic model developed for the responses, color removal and energy consumption, can be used for prediction.

CONFLICT OF INTEREST

The authors have declared no conflict of interest.

SUPPLEMENTARY MATERIAL

The Supplementary Material for this paper is available online at https://dx.doi.org/10.2166/wst.2020.151.

REFERENCES

APHA, AWWA & WEF 1995 *Standard Methods for the Examination of Water and Wastewater*, 19th edn. American Public Health Association/American Water Works Association/Water Environment Federation, Washington, DC, USA.

Awad, H. S. & Galwa, N. A. 2005 Electrochemical degradation of Acid Blue and Basic Brown dyes on Pb/PbO_2 electrode in the presence of different conductive electrolyte and effect of various operating factors. *Chemosphere* **61** (9), 1327–1335. doi:10.1016/j.chemosphere.2005.03.054.

Baddouh, A., Bessegato, G. G., Rguiti, M. M., El Ibrahimi, B., Bazzi, L., Hilali, M. & Zanoni, M. V. 2018 Electrochemical decolorization of Rhodamine B dye: influence of anode material, chloride concentration and current density. *Journal of Environmental Chemical Engineering* **6** (2), 2041–2047. doi:10.1016/j.jece.2018.03.00.

Bedolla-Guzman, A., Sirés, I., Thiam, A., Peralta-Hernández, J. M., Gutiérrez-Granados, S. & Brillas, E. 2016 Application of anodic oxidation, electro-Fenton and UVA photoelectro-Fenton to decolorize and mineralize acidic solutions of Reactive Yellow 160 azo dye. *Electrochimica Acta* **206**, 307–316. doi:10.1016/j.electacta.2016.04.166.

Canizares, P., Saez, C., Lobato, J. & Rodrigo, M. A. 2004 Electrochemical oxidation of polyhydroxybenzenes on boron-doped diamond anodes. *Industrial & Engineering Chemistry Research* **43** (21), 6629–6637.

Canizares, P., Lobato, J., Paz, R., Rodrigo, M. A. & Saez, C. 2005 Electrochemical oxidation with phenolic wastes with boron-doped diamond anodes. *Water Research* **39** (12), 2687–2703.

Chen, X., Chen, G. & Yue, P. L. 2003 Anodic oxidation of dyes at novel Ti/B-diamond electrodes. *Chemical Engineering Science* **58** (3–6), 995–1001. doi:10.1631/jzus.2007.A1457.

Comninellis, C. & Chen, G. 2010 *Electrochemistry for the Environment*, Springer, New York, USA.

Comninellis, C. & Pulgarin, C. 1993 Electrochemical oxidation of phenol for wastewater treatment using SnO_2 anodes. *Journal of Applied Electrochemistry* **23**, 108–112.

Esquivela, K., Arriaga, L. G., Rodriguez, F. J., Martinez, L. & Godinez, L. A. 2009 Development of a TiO_2 modified optical fiber electrode and its incorporation into a photoelectrochemical reactor for wastewater treatment. *Water Research* **43** (14), 3593–3603.

Fajardo, A., dos Santos, A., Costa, E., Silva, D. & Martinez-Huitle, C. 2019 Effect of anodic materials on solar photoelectro-Fenton process using a diazo dye as a model contaminant. *Chemosphere* **225**, 880–889. https://doi.org/10.1016/j.chemosphere.2019.03.071.

Forgacs, E., Cserhati, T. & Oros, G. 2004 Removal of synthetic dyes from wastewaters: a review. *Environment International* **30**, 953–971. doi:10.1016/j.envint.2004.02.001.

Gherardini, L., Michaud, P. A., Panizza, M., Comninellis, C. & Vatistas, N. 2001 Electrochemical oxidation of 4-chlorophenol for wastewater treatment: definition of normalized current efficiency. *Journal of the Electrochemical Society* **148** (6), D78–D82.

Gutierrez, M. C. & Crespi, M. 1999 A review of electrochemical treatments for colour elimination. *Coloration Technology* **115** (11), 342–345. doi:10.1111/j.1478-4408.1999.tb00323.x.

Hao, O. J., Kim, H. & Chiang, P. C. 2000 Decolorization of wastewater. *Critical Reviews in Environmental Science and Technology* **30** (4), 449–505. doi: 10.1080/10643380091184237.

Iranpour, F., Pourzamani, H., Mengelizadeh, N., Bahrami, P. & Mohammadi, H. 2018 Application of response surface methodology for optimization of reactive black 5 removal by three dimensional electro-Fenton process. *Journal of Environmental Chemical Engineering* **6** (2), 3418–3435. doi:10.1016/j.jece.2018.05.023.

Kawagoe, K. T. & Johnson, D. C. 1994 Electrocatalysis of anodic oxygen-transfer reaction. Oxidation of phenol and benzene at bismuth-doped lead dioxide electrodes in acidic solutions. *Journal of the Electrochemical Society* **141**, 3404–3409.

Kötz, R., Stucki, S. & Carcer, B. 1991 Electrochemical waste water treatment using high overvoltage anodes. Part I: Physical and electrochemical properties of SnO_2 anodes. *Journal of Applied Electrochemistry* **21** (1), 14–20. doi:10.1007/BF01103823.

Li, Z., Yuan, S., Qiu, C., Wang, Y., Pan, X., Wang, J., Wang, C. & Zuo, J. 2013 Effective degradation of refractory organic pollutants in landfill leachate by electro-peroxone treatment. *Electrochimica Acta* **102**, 174–182. https://doi.org/10.1016/j.electacta.2013.04.034.

Martínez-Huitle, C. A. & Panizza, M. 2018 Electrochemical oxidation of organic pollutants for wastewater treatment. *Current Opinion in Electrochemistry* **11**, 62–72. doi:10.1016/j.coelec.2018.07.010.

Martínez-Huitle, C. A. & Brillas, E. 2009 Decontamination of wastewaters containing synthetic organic dyes by electrochemical methods: a general review. *Applied Catalysis B: Environmental* **87**, 105–145. doi:10.1016/j.apcatb.2008.09.017.

Mohan, N. & Bala Subramanian, N. 2006 In situ electrocatalytic oxidation of acid violet 12 dye effluent. *Journal of Hazardous Materials* **136** (2), 239–243. doi:10.1016/j.jhazmat.2005.11.074.

Mohan, N., Bala Subramanian, N. & Subramanian, V. 2001 Electro chemical treatment of simulated textile effluent. *Chemical Engineering & Technology* **24** (7), 749–753. doi:10.1002/1521-4125(200107).

Moradi, F. & Dehghanian, C. 2014 Addition of IrO_2 to $RuO_2 + TiO_2$ coated anodes and its effect on electrochemical performance of anodes in acid media. *Progress in Natural Science: Materials International* **24** (2), 134–141.

Naim, M. M. & El Abd, Y. M. 2002 Removal and recovery of dyestuffs from dyeing wastewaters. *Separation and Purification Methods* **31** (1), 171–228. doi:10.1081/SPM-120006116.

Panizza, M. & Cerisola, G. 2009 Direct and mediated anodic oxidation of organic pollutants. *Chemical Reviews* **109**, 6541–6569. https://doi.org/10.1021/cr9001319.

Rajkumar, D. & Kim, J. G. 2006 Oxidation of various reactive dyes with in situ electro-generated active chlorine for textile dyeing industry wastewater treatment. *Journal of Hazardous Materials* **136** (2), 203–212. doi:10.1016/j.jhazmat.2005.11.096.

Rajkumar, K. & Muthukumar, M. 2012 Optimization of electro-oxidation process for the treatment of Reactive Orange 107 using response surface methodology. *Environmental Science and Pollution Research* **19** (1), 148–160. doi:10.1007/s11356-011-0532-2.

Robinson, T., McMullan, G., Marchant, R. & Nigam, P. 2001 Remediation of dyes in textile effluent: a critical review on current treatment technologies with a proposed alternative. *Bioresource Technology* **77**, 247–255. doi: 10.12691/ajmr-1-4-3.

Rocha, J. H., Solano, A. M., Fernandes, N. S., da Silva, D. R., Peralta-Hernandez, J. M. & Martínez-Huitle, C. A. 2012 Electrochemical degradation of Remazol Red BR and NovacronBlue CD dyes using diamond electrode. *Electrocatalysis* **3** (1), 1–2.

Simond, O., Schaller, V. & Comninellis, C. 1997 Theoretical model for the anodic oxidation of organics on metal oxide electrodes. *Electrochimica Acta* **42** (13–14), 2009–2012. doi:10.1016/S0013-4686(97)85475-8.

Stucki, S., Kötz, R., Carcer, B. & Suter, W. 1991 Electrochemical waste water treatment using high overvoltage anodes part II: anode performance and applications. *Journal of Applied Electrochemistry* **21** (2), 99–104. doi:10.1007/BF01464288.

First received 8 January 2020; accepted in revised form 23 March 2020. Available online 3 April 2020